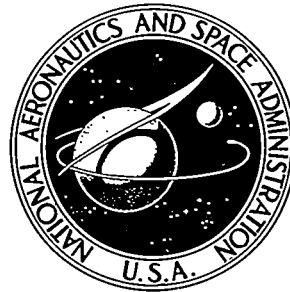


NASA TECHNICAL NOTE



NASA TN D-5705

C.1

NASA TN D-5705



LOAN COPY: RETURN TO  
AFWL (WLOL)  
KIRTLAND AFB, N MEX

# EFFECTS OF VORTEX SHEDDING ON FUEL SLOSH DAMPING PREDICTIONS

*by Henry A. Cole, Jr.*

*Ames Research Center  
Moffett Field, Calif.*

NATIONAL AERONAUTICS AND SPACE ADMINISTRATION • WASHINGTON, D. C. 20546



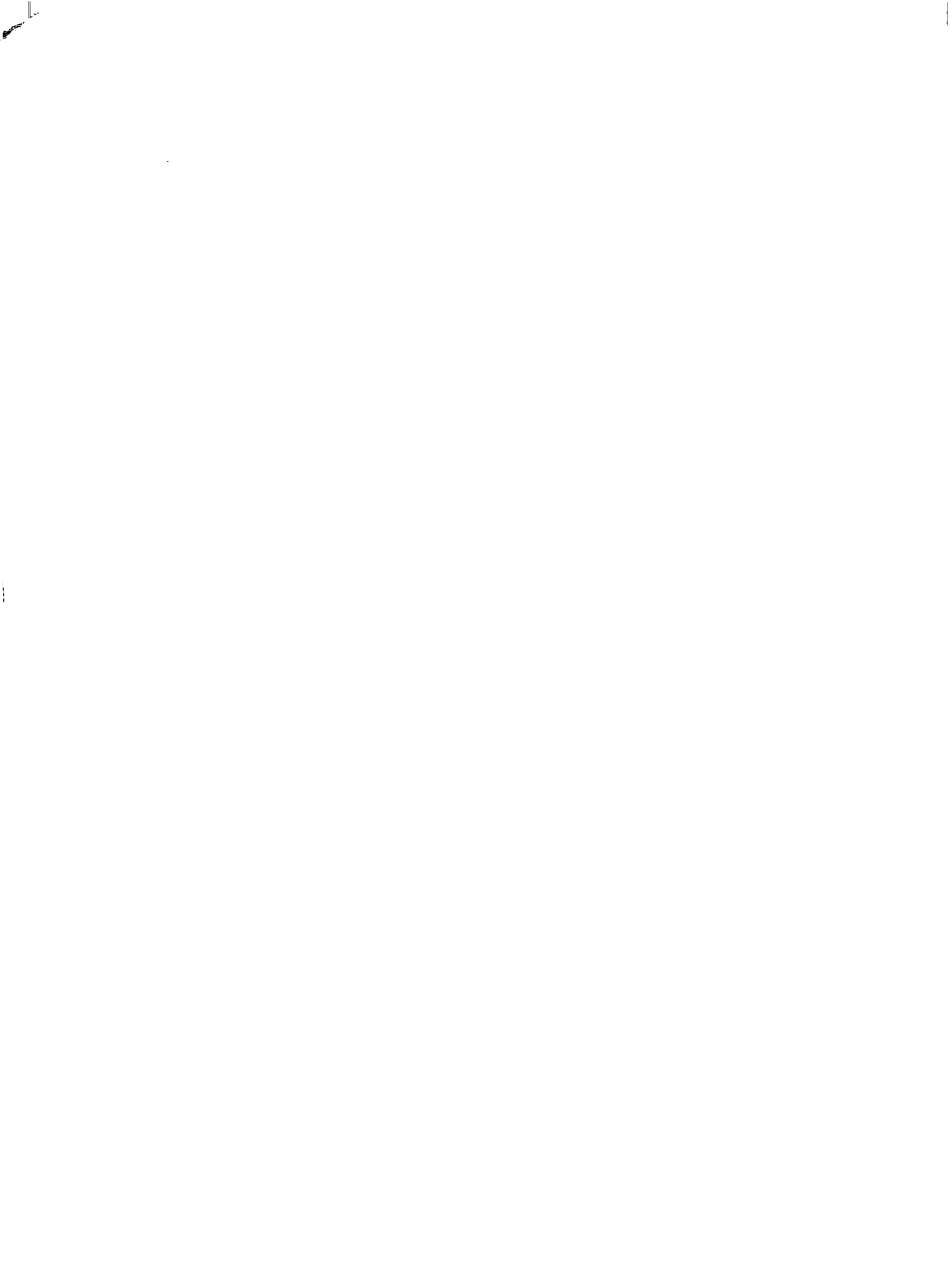
0761



0131529

1. Report No. NASA TN D-5705	2. Government Accession No.	3. Recipient's Catalog No.	
4. Title and Subtitle EFFECTS OF VORTEX SHEDDING ON FUEL SLOSH DAMPING PREDICTIONS		5. Report Date March 1970	
		6. Performing Organization Code	
7. Author(s) Henry A. Cole, Jr.		8. Performing Organization Report No. A-3322	
9. Performing Organization Name and Address NASA Ames Research Center Moffett Field, Calif., 94035		10. Work Unit No. 124-08-05-08-00-21	
		11. Contract or Grant No.	
		13. Type of Report and Period Covered  Technical Note	
12. Sponsoring Agency Name and Address National Aeronautics and Space Administration Washington, D.C. 20546		14. Sponsoring Agency Code	
15. Supplementary Notes			
16. Abstract  Predictions of fuel slosh damping by ring baffles in cylindrical tanks are shown to differ from experimental measurements by as much as 100 percent over a range of tank diameters from 12 to 112 inches, oscillation amplitudes from 0.1 to 1.5 baffle widths, and baffle depths of 0.3 to 0.5 tank radius. Agreement between experiments and predictions is brought to within 20 percent when corrections are included for transitional flow due to vortex shedding, generalized mass change due to translation, and wall damping.			
17. Key Words Suggested by Author Fuel slosh Damping Vortex Oscillation Stability		18. Distribution Statement Unclassified - Unlimited	
19. Security Classif. (of this report) Unclassified	20. Security Classif. (of this page) Unclassified	21. No. of Pages 28	22. Price* \$3.00

\*For sale by the Clearinghouse for Federal Scientific and Technical Information  
Springfield, Virginia 22151



## SYMBOLS

- A baffle double amplitude, ft
- $A_{\text{eff}}$  double amplitude of vortex, in y direction, ft
- a cylindrical tank radius, ft
- $a_1$  amplitude of fundamental-frequency baffle force in phase with velocity, lb
- $C_D$  equivalent viscous drag coefficient,  $\frac{3\pi a_1}{\rho S(A\omega)^2}$  (ref. 5)
- $C_{D_0}$  drag coefficient used for comparison (fig. 7)
- $C_f$  correction factor for damping ratio equations (fig. 7)
- d depth of baffle measured from quiescent liquid surface, ft
- F baffle force, lb
- g acceleration of gravity, ft/sec<sup>2</sup>
- h depth of fluid, ft
- i  $\sqrt{-1}$
- k  $\frac{1.84}{a}$  (ref. 3)
- $l$  radial distance from vortex
- m generalized mass in fundamental mode of fluid in tank without baffle, slugs
- $m_c$  generalized mass in fundamental mode of fluid in tank with baffle, slugs
- $m_t$  mass of tank, slugs
- n acceleration of vehicle, g
- $\bar{Re}$  baffle mean Reynolds number,  $\frac{2\bar{V}w}{\nu}$
- r polar coordinate in  $\xi$  plane, plate widths

$S$	baffle area
$T$	period of oscillation, sec
$t$	time, sec
$u_{\theta}$	tangential component of velocity at radius $r$ , units of $V$
$u_r$	radial component of velocity, units of $V$
$V$	vertical velocity of plate, ft/sec or plate widths/sec
$\bar{V}$	mean free-stream velocity (over one cycle of oscillation) of baffle edge relative to fluid, ft/sec
$V_s$	velocity of sound, ft/sec
$w$	plate width, ft
$x$	horizontal coordinate in complex $z$ plane, plate widths (fig. 8)
$y$	vertical (imaginary) coordinate in complex $z$ plane, plate widths (fig. 8)
$y_s$	surface wave amplitude at the wall, ft
$\Gamma$	circulation of vortex
$\zeta$	ratio of damping to critical damping
$\zeta_0$	damping ratio due to wall damping and any tare damping
$\theta$	polar coordinate in $\xi$ plane, and in cylindrical tank
$\nu$	kinematic viscosity, ft <sup>2</sup> /sec
$\rho$	mass density, slugs/ft <sup>3</sup>
$\omega$	frequency of forced oscillation, rad/sec
$\omega_n$	first natural undamped frequency of fluid with tank fixed, rad/sec
$\omega_c$	coupled natural undamped frequency of tank and fluid with tank free to translate, rad/sec
$\xi$	complex plane used in conformal transformation (fig. 8)



## Subscripts

meas measured

pred predicted

i related to vortex i

# EFFECTS OF VORTEX SHEDDING ON FUEL

## SLOSH DAMPING PREDICTIONS

By Henry A. Cole, Jr.

Ames Research Center

### SUMMARY

Predictions of fuel slosh damping by ring baffles in cylindrical tanks are shown to differ from experimental measurements by as much as 100 percent over a range of tank diameters from 12 to 112 inches, oscillation amplitudes from 0.1 to 1.5 baffle widths, and baffle depths of 0.3 to 0.5 tank radius. Agreement between experiments and predictions is brought to within 20 percent when corrections are included for transitional flow due to vortex shedding, generalized mass change due to translation, and wall damping.

### INTRODUCTION

One of the perplexing problems in predicting fuel slosh damping by ring baffles in cylindrical tanks has been that some experiments (refs. 1, 2, and 3) have shown good agreement with the prediction method of Miles (ref. 4) whereas other experiments (refs. 5, 6, and 7) have shown significant deviations. In the past, much of this difference has been attributed to experimental scatter. More recently, some general reviews have been made to see if predictions could be made over a wider range of conditions, high gravity (ref. 8) and low gravity (ref. 9). These reports indicate that additional factors are needed when the prediction method of Miles is applied outside the range of the original data.

The prediction method of Miles was based on a strip theory integration using the two-dimensional data from reference 10 and the potential flow velocities of the first asymmetrical mode in a cylindrical tank. A similar method, also based on strip theory, was developed about the same time (ref. 5). These prediction methods differed primarily in the two-dimensional data on which they were based. The data of Keulegan and Carpenter used in Miles' theory were obtained by measuring the forces on a plate while the fluid was oscillated in a rectangular tank of fixed dimensions; hence the frequency of oscillation was fixed. The method of reference 5 used force measurements on a plate mounted to a curved wall, which was driven about a fixed pivot point over a range of frequencies and amplitudes. The former method indicated that the drag coefficient of an oscillating plate depends on a period parameter which is proportional to the ratio of the oscillation amplitude to the plate width. The latter method indicated, in addition to the amplitude width ratio, that the drag coefficient varied with velocity. In reference 8, the two-dimensional experiments were shown to be reasonably consistent when Cauchy

number was included in the equations. The two experiments, however, covered different ranges of amplitudes and had only a small overlap.

The exceptionally high drag coefficients used in these theories should be of considerable interest to fluid dynamicists. At small amplitudes, the drag coefficient may be 25 times or more larger than the steady-state value. The drag coefficients are usually given in an equivalent viscous drag coefficient form that results in the same energy loss in a cycle of oscillation as the actual measured values. The actual damping force is quite nonlinear and at the maximum velocity point the instantaneous drag coefficient is usually much larger than the equivalent viscous coefficient. These exceptionally high drag coefficients are apparently due to the proximity of the shed vortices to the plate and are quite sensitive to small changes in velocity at the baffle edge. A slight thickening (ref. 5) of the baffle can cause a large drop in the coefficient, and flexibility (ref. 7) can cause a large increase. In view of this sensitivity, small variations in the waveform may also have large effects on the damping effectiveness of baffles in the small amplitude region. One such variation is the waveform induced by the sloshing surface wave when a baffle is located on the sidewall of a tank. This varies from a sine wave in that the maximum velocity in the upward direction is greater than the velocity in the downward direction. This and other variations in surface waveform may account for deviations of experimental results from the theoretical predictions.

During a recent review, it was decided to make a systematic study of the data to see if some missing factors in the prediction methods could be found. Experimental damping measurements from a range of tank diameters from 12 to 112 inches were selected from references 6, 7, and 8. The study was limited to measurements using the wave decay method (in order to avoid variations due to the method of measuring damping), to thin baffles (in accordance with ref. 11), and to baffle depths of 0.3 tank radius and greater (to minimize surface effects). In addition, the possibilities of waveform effect on the drag coefficients mentioned above was studied by comparing ink trace patterns of the shed vortices for a sinusoidal waveform and the waveform induced by the sloshing surface wave. The ink trace experiments are very useful in the oscillating plate problem because a large part of the drag is induced by the vortex shedding and changes in the flow pattern can be interpreted as changes in the drag.

#### COMPARISON OF MEASURED AND PREDICTED RING DAMPING

The comparison of the measured and the predicted damping for various tank sizes is shown in figure 1 for Miles' equation and figure 2 for the method of reference 8. Figure 1(a) compares Miles' equation in its original form with the data; figures 1(b) through (d) show Miles' equation modified as noted. Similarly, figure 2(a) is based on the unmodified equation of reference 8, while figures 2(b) and (c) show the result of modifications.

The data used for these comparisons (table 1) were restricted to baffle depths where surface effects could be considered small. This was done by

noting the depth in reference 1 at which the frequency with and without baffles nearly coincided. This was interpreted to mean that the surface wave-form is not affected by the baffle and that the assumption of potential flow in the equations is valid. Miles' equation predicts damping ratio as follows:<sup>1</sup>

$$\zeta = 3 \left[ 1 - \left( \frac{a-w}{a} \right)^2 \right]^{3/2} \exp \left( -4.60 \frac{d}{a} \right) \left( \frac{y_s}{a} \right)^{1/2} \quad (1)$$

As may be seen in figure 1(a), the measured damping ratio exceeds the predictions by as much as 100 percent and falls below by as much as 30 percent.

Reference 8 gives the equation:

$$\zeta_{\text{pred}} = \zeta_0 + 0.9 \left( \frac{V_s^2}{\text{ang}} \right)^{1/8} \left( \frac{w}{a} \right)^{1.4} \left( 1 - \frac{w}{2a} \right) \left( \frac{y_s}{a} \right)^{0.35} \exp \left( -4.3 \frac{d}{a} \right) \quad (2)$$

It is seen in figure 2(a) that this equation agrees well with the data at large amplitudes, but falls below by as much as 60 percent at small amplitudes.

#### Wall Damping

One of the main differences between the two prediction methods is the inclusion of the wall damping ( $\zeta_0$ ). That it should be included seems reasonable because the wall damping can become a significant percentage of the total damping, particularly in small tanks and at large amplitudes in any size tank. If wall damping is included in Miles' equation, it becomes

$$\zeta_{\text{pred}} = \zeta_0 + 3 \left[ 1 - \left( \frac{a-w}{a} \right)^2 \right]^{3/2} \exp \left( -4.60 \frac{d}{a} \right) \left( \frac{y_s}{a} \right)^{1/2} \quad (3)$$

which is compared with the experimental data in figure 1(b). The agreement now is much better at large amplitudes, but not quite as good at low amplitudes. The systematic deviation of the measurements from the prediction indicates that the theory needs further modification. The wall damping included in figures 1(b) and 2(a) was not given in some of the reports, in which case it was calculated by the method of reference 12.

#### Generalized Mass

The mass used for calculating the damping ratio in equations (1) and (2) is the generalized mass of the fundamental sloshing mode of the fluid in a fixed tank without baffles. In the real sloshing situation, some of the sloshing mass is retarded by the baffle. This effect is known to fluid

---

<sup>1</sup>Some experimenters use a coefficient of 2.83, which is obtained by calculating Miles' equation 11(a) to three significant figures. However, if one also calculates Miles' equation (7) exactly by allowing  $C_D$  to vary around the ring, the coefficient becomes 3.04. The original rounded off value of 3 is used here for comparison.

dynamicists as additional apparent mass, which is usually added to the mass of an object moving in a fluid. In this case, it has to be subtracted since the baffle is fixed and the mass of fluid is moving. Another reduction in the generalized mass relative to the fixed tank value is needed when a tank is given freedom in translation. When the tank is fixed, the center of gravity of the fluid moves from side to side. When the tank is free to move in translation, the center of gravity tends to stay fixed with the result that the generalized mass of sloshing decreases. Modifications for these effects are developed in this section.

In the measurements of reference 5, the additional apparent mass of the baffle was found to be from 0.7 to 1 times the mass of a semicircle of fluid of radius  $w$  except when the baffle was near the surface. If the form of the surface wave is assumed to be unaffected by the baffle (maximum potential energy constant), the generalized mass (ref. 5) to be used in calculating the damping ratio is modified by the factor

$$\frac{m_c}{m} = \frac{1.84\pi}{[1 - (ka)^{-2}]^2} \left(\frac{y}{y_s}\right)^2 \left(\frac{\omega_c}{\omega_n}\right)^2 \left(\frac{w}{a}\right)^2 \left(1 - 0.4 \frac{w}{a}\right) \quad (4)$$

where  $\omega_c/\omega_n$  has been introduced to account for the difference in frequency of a fixed tank and one free in translation. The correction for additional apparent mass of the baffle proved to be less than 2 percent of the damping ratio for the size and depth of baffles in this report. For larger baffles, this effect could be significant.

The effect of tank translation is another matter. As given in reference 13, when the tank is free, it moves in translation so as to minimize the movements of the center of gravity of the system as a whole, and the frequency of fuel sloshing is increased. It becomes

$$\omega_c = \frac{\omega_n}{\sqrt{1 - \frac{2 \tanh 1.84(h/a)}{1.84(h/a)(1.84^2 - 1)(1 + m_t/m)}}} \quad (5)$$

The damping force as used in equation (3) varies as the frequency squared, and equation (3) becomes:

$$\zeta = \zeta_0 + 3 \left[1 - \left(\frac{a-w}{a}\right)^2\right]^{3/2} \exp\left(-4.60 \frac{d}{a}\right) \left(\frac{y_s}{a}\right)^{1/2} \left(\frac{\omega_c}{\omega_n}\right)^2 \quad (6)$$

This result (eq. (6)) is shown compared with experiment in figure 1(c). The large amplitude tests of reference 8 were made with a tank free in translation. It had a fuel slosh frequency of 6.9 rad/sec when free compared to the tank-fixed frequency of 6.3 rad/sec. The agreement at large amplitudes, with this modification, is fairly good, but the tendency of the theory to overestimate at low amplitudes persists.

A similar correction may be applied to equation (2) (ref. 8). In this case,  $\zeta$  varies as fuel slosh frequency to the 1.75 power, and equation (2) becomes

$$\zeta = \zeta_0 + 0.9 \left( \frac{V_s^2}{\text{ang}} \right)^{1/8} \left( \frac{w}{a} \right)^{1.4} \left( 1 - \frac{w}{2a} \right) \left( \frac{y_s}{a} \right)^{0.35} \exp \left( -4.3 \frac{d}{a} \right) \left( \frac{\omega_c}{\omega_n} \right)^{1.75} \quad (7)$$

This equation, with  $\omega_c/\omega_n$  from equation (5), is compared with experiment in figure 2(b). Here, too, the agreement is good at large amplitudes, but the trend to overprediction at small amplitudes is apparent.

## FLOW VISUALIZATION STUDIES

Further studies were undertaken in an effort to explain the discrepancy between the theories and measurements at small amplitudes. Since the prediction methods are based on the two-dimensional drag measurements of references 5 and 10, the vortex flow patterns in two-dimensional flow were studied over a range of amplitude width ratios. This was done by introducing ink at the edge of a 3-inch plate mounted on the sidewall of the tank of reference 5 and photographing the vortex paths.<sup>2</sup> Flow was induced by two methods: (1) The plate was driven in pure sinusoidal translation. (2) A sloshing motion was set up in the tank with the plate stationary. The vortex paths were used to deduce the drag force on the plate. This method was applied in reference 11 to show the effect of plate thickness on the effective damping. The method of deducing the forces on a plate from the shed vortices is well known. Von Kármán obtained the drag of a flat plate in steady flow by taking measurements of the vortex street (ref. 14). Airfoil flutter theory (ref. 15) is also based on analysis of the shed vortices and the velocities which they induce on the airfoil.

The two-dimensional drag measurements on which equations (1) and (2) are based were obtained for essentially sinusoidal motion. In the first, the fluid was moved and the baffle was fixed; in the second, the baffle was moved and the fluid was fixed at the boundaries. The dependence of the unsteady drag on whether the fluid or the baffle moves is treated in reference 9; it is concluded that for a plate, only the relative motion matters. This is supported by figures 1(c) and 2(b): the theory in figure 1(c) is based on data in which the fluid was moved, while the theory of figure 2(b) was based on data for which the plate was moved; both show similar trends of variation with  $A/w$ . However, the motion of the fluid over a baffle mounted on a sidewall is by no means sinusoidal, but is rather a skew motion in which the up amplitude is greater than the down amplitude (ref. 10), and the question arises as to whether or not this difference in relative motion could affect the drag.

In the present observations of vortex patterns, flow patterns were obtained for sinusoidal motion by driving the plate mounted on a sliding wall with the fluid fixed at the surface by a tank cover, and for slosh motion by driving the surface wave with the baffle fixed to the sidewall (see fig. 3). Both were done at a  $d/a$  of 0.5. The results of the ink traces of the vortex paths are shown on figure 4 for two amplitude width ratios. It should be

---

<sup>2</sup>Ink trace experiments were conducted by William E. Moritz.

noted that in the sinusoidal motion the plate edge moved up and down vertically, in contrast to the slosh motion, which approximately followed the theoretical potential flow streamline shown. For  $A/w = 1$ , the vortex paths are quite similar except for a slight rotation of the paths due to the difference in the velocity direction. The distances traveled by the vortices in a cycle and their distance apart is nearly the same for the two motions indicating that the drag forces were approximately the same.

For the smaller amplitude,  $A/w = 0.33$ , a startling change takes place. The slosh motion results in a nonsymmetrical pattern similar to the one at the larger amplitude, but the sinusoidal motion results in a nearly symmetrical pattern in which the amplitude of the vortices exceeds the motion of the plate by 50 percent. This result may explain the poor agreement of the predictions at low amplitudes shown in figures 1 and 2. Apparently at small amplitudes, the flow pattern of a plate in sinusoidal motion on which the prediction methods are based differs from the flow pattern which actually exists with the fuel sloshing type of motion. The slosh motion depends on baffle depth and some experiments were run at varying depths. Further changes in the flow pattern were observed as the baffle approached the surface. Over the range of depths considered in this report, however, the flow patterns were nearly identical.

Typical frames of the 16mm film of the vortex shedding are shown in figure 5 for  $A/w = 0.33$  where the significant change in flow pattern occurs. Figures 5(a) and (b) show the upward moving vortex after half a cycle for sinusoidal motion and slosh motion, respectively. The amplitude of the baffle can be seen for the sinusoidal motion on the 1-inch background grid; for slosh motion the amplitude was calibrated by introducing ink in the tank without the baffle and measuring the surface wave amplitude needed to give the correct amplitude at the baffle location. The effective amplitude of the vortex can be seen to be about 1-1/2 inches in figure 5(a) and about 1 inch in figure 5(b).

Figures 5(c) and (d) show the downward moving vortices at the end of a complete cycle. For sinusoidal motion it may be seen that the vortex pattern is similar to the upward moving vortex in figure 5(a). For slosh motion, the flow pattern is entirely different with the vortex pair swimming rapidly away from the baffle in a nonsymmetrical pattern.

### Drag Coefficients

The consequences of the above observations may be clearly seen in figure 6 which shows the drag coefficients from references 5, 10, and 16 plotted versus  $A/w$ . The figure shows the data obtained by Keulegan and Carpenter and the curve fitting by Miles' equations. Note that the data do not extend into the region of amplitudes for which Miles' equation has been so extensively applied. Figure 6 also shows the range of values from reference 5. These data were obtained at constant  $A/w$  over a range of velocities, whereas the Keulegan and Carpenter data were taken essentially at constant velocity. The effect of fuel slosh motion on the drag coefficient curve, shown by the dashed curve, is estimated in the appendix. The pendulum

experiments of reference 16 show a similar transition in the drag curve. From this figure, it would not be expected that Miles' equation would apply accurately below  $A/w = 1$ .

On figure 6(b), the relation of the data to the drag coefficient expression from reference 8 is shown. For the same conditions as tested by Keulegan and Carpenter ( $T = 2$  sec,  $w = 1-1/2$  to  $3/4$  inch) the predicted values are about 20 percent higher but have the same slope as the data. The predicted transition due to slosh motion of the 3-inch,  $T = 1$  sec curve (derived in the appendix) is shown. A complete solution cannot be given because the dependence of the drag coefficient on the flow velocity has not been established for this transitional flow regime. Therefore, the correction factor given in figure 6 should not be applied at conditions too far removed from the test conditions on which they are based.

### Prediction of Damping in Cylindrical Tanks

A correction factor for Miles' equation and the equation of reference 8 is shown in figure 7. It was obtained by using the slosh-motion drag coefficients estimated and shown in figure 6, and correcting for all approximations in the derivation of the damping equations including variation of  $C_D$  with amplitude around the ring. The ratio  $C_D/C_{D_0}$  shown in the integrals is the ratio of the drag coefficient from the estimated curve as it varies around the ring to the constant drag coefficients used in deriving equations (1) and (2). An approximate correction may be introduced by multiplying the equations by the factors shown. The effect of the correction factors on the results is shown in figures 1(d) and 2(c), respectively. It may be seen that the agreement between experiment and theory is improved considerably and falls within a range that can be attributed to experimental scatter.

The sensitivity of the induced drag to the small variation in fluid motion shown here offers an explanation for the variations in two-dimensional drag coefficients measured by various experimenters (refs. 5, 10, and 16) in the  $A/w = 1$  to  $1/4$  region. It is difficult to say which of these measurements most closely represents the actual vortex motion in a cylindrical tank. The two-dimensional experiments have a straight vortex line whereas the vortex line in the cylindrical tank is curved. Also, in cylindrical tank experiments there is usually some excitation of the first symmetrical mode, which also alters the velocity at the baffle. These variations in velocity and geometry would have to be taken into account to predict the damping more exactly.

### CONCLUSIONS

On the basis of comparisons of measured and predicted damping of fuel sloshing by the ring baffles in cylindrical tanks, and study of patterns of vortex shedding of oscillating plates in sinusoidal and in fuel sloshing motion, it is concluded that:

1. A transitional flow occurs at amplitude-to-width ratios of less than one, in which the vortex pattern can be symmetric or nonsymmetric depending on whether the motion is sinusoidal or surface-induced sloshing motion at a tank side wall. The change in flow pattern can cause changes of damping effectiveness of the order of 50 percent.

2. Prediction of damping of fuel sloshing by ring baffles should include wall damping (tare damping), a correction for generalized mass if the tank is not fixed, and a correction for slosh motion for amplitude-to-width ratios of less than one.

Ames Research Center  
National Aeronautics and Space Administration  
Moffett Field, Calif. 94035, Nov. 25, 1969

## APPENDIX A

### MEASUREMENT OF DRAG FROM THE VORTEX PATH

A quantitative measure of the drag associated with the various vortex patterns was obtained by means of the well-known relations of force induced on the plate due to vortices in the fluid (ref. 15). The equation

$$F(t) = \rho \frac{d}{dt} \sum \Gamma_i x_i \quad (A1)$$

expresses the relation of the induced force on the plate to the location and strength of the vortices. A complete integration of the force over an oscillation cycle was considered beyond the scope of the present report. To simplify the calculation, it was assumed that the maximum force occurs when the flow or baffle velocity is a maximum and that  $\Gamma_i$  may be treated as constant in taking the derivatives indicated in equation (A1). Then

$$F_{\max} = \rho \sum \Gamma_i \left. \frac{dx_i}{dt} \right|_{v_{\max}} \quad (A2)$$

in which the  $\Gamma_i$  are evaluated at the maximum velocity point by transforming the flat plate and vortex path into a unit circle and corresponding vortex path by the conformal transformation shown in figure 8. This is the same as the usual Joukowski transformation except that the  $z$  coordinate is multiplied by 2 so that the plate width equals the radius of the circle. This procedure enables one to satisfy the condition of no flow through the boundary by putting an image vortex of  $\Gamma_1$ , for example, at  $(1/r_1, \theta_1)$  and images on the other side of the wall as shown. The path of the vortex  $\Gamma_1$  starts on the diagram at  $t = 0$  and reaches the maximum velocity point at  $t = \pi/2\omega$ . The second vortex  $\Gamma_2$  forms at  $t = \pi/\omega$  and reaches the point  $(r_2, \theta_2)$  at  $t = 3\pi/2\omega$ . The velocities induced by the vortices were calculated by the relation

$$V_i = \frac{\Gamma_i}{2\pi l_i} \quad (A3)$$

where  $l_i$  is the radial distance from the vortex and  $V_i$  is the velocity normal to  $l_i$ .

The velocity at a point in the fluid due to flow around the circle is

$$\left. \begin{aligned} u_\theta &= V \cos \theta \left( 1 + \frac{1}{r^2} \right) \\ u_r &= V \sin \theta \left( 1 - \frac{1}{r^2} \right) \end{aligned} \right\} \quad (A4)$$

In calculating the strength of the vortices, the usual procedure is to satisfy the Kutta condition at the plate edge. In airfoil theory, this procedure was based on the observation that the airflow was tangent to the trailing edge. In the vertically moving plate, the conditions to be satisfied at

the plate edge could not be accurately observed by the ink trace patterns. However, the vortex paths at the points of maximum velocity were well defined and were used for calculating the vortex strengths.

For the nonsymmetrical flow pattern, velocities were resolved by means of the above relations as shown in figure 9. The solution was obtained graphically by assuming a unit strength for each vortex, and resolving the velocity at the path due to the vortices and their images for this and the previous cycle. The vortices from the previous cycle had little effect because they were close together and would swim far from the baffle before the next pair formed. When the resolved velocities were obtained for the unit vortices at  $(r_1, \theta_1, \pi/2\omega)$  and  $(r_2, \theta_2, 3\pi/2\omega)$ , the relative strengths of  $\Gamma_1$  and  $\Gamma_2$  were determined that produced a velocity tangent to the observed paths. For  $t = \pi/2\omega$ , the velocity induced is primarily due to  $\Gamma_1$ , so that  $\Gamma_1$  may be determined directly as shown in figure 9(a). At  $t = 3\pi/2\omega$ , since  $\Gamma_1$  is known, the strength of  $\Gamma_2$  may be determined by resolution as shown in figure 9(b). The calculation was well conditioned and indicated that the lower vortex  $\Gamma_2$  was much stronger than  $\Gamma_1$ .

In the symmetrical case, figure 10, the upper and lower vortices are of nearly the same strength, and velocities need be resolved only at one point. This flow pattern is quite different in that the vortex pairs do not swim rapidly off, and hence, the vortices from the previous cycle strongly influence the force on the plate. The large velocity component from  $\Gamma_2$  carries  $\Gamma_1$  to an amplitude 50 percent higher than the motion of the plate shown in figure 4.

Any flow patterns that fall between the symmetrical and nonsymmetrical cases reduce essentially to two simultaneous equations in two unknowns and may be solved graphically.

Some of the image vortices had secondary effects on the graphical solution of the vortex strengths. By neglecting these, an equation for drag coefficient was developed as follows. It was assumed that the strengths of  $\Gamma_1$  and  $\Gamma_2$  were determined by setting the velocity due to the first image in the unit circle equal to the velocity component  $u_\theta$ . This gives

$$\Gamma_i = 4\pi V \left( r_i - \frac{1}{r_i} \right) \left( 1 + \frac{1}{r_i^2} \right) \cos \theta_i \quad (A5)$$

It should be noted that  $2V$  is used as the velocity since the scale of the transformation is 2 at infinity.

The  $dx/dt$  was approximated by measuring the  $\Delta x$  that occurs in half a cycle as shown in figure 4. That is

$$\frac{dx}{dt} \approx \frac{\Delta x_i \omega}{\pi} \quad (A6)$$

Substituting equations (A5) and (A6) in equation (A2)

$$F_{\max} \approx 4\rho V \omega r_i \left( 1 - \frac{1}{r_i^4} \right) \Delta x_i \cos \theta_i \quad (A7)$$

where  $V = A\omega/2w$ .

Taking an average of first and second halves of the cycle and putting in coefficient form by dividing by  $\rho V^2/2$ , we obtain

$$C_{D_{\max}} \approx \frac{8}{A/w} \left( \frac{A_{\text{eff}}}{A} \right)^2 \left[ r_1 \left( 1 - \frac{1}{r_1^4} \right) \Delta x_1 \cos \theta_1 + r_2 \left( 1 - \frac{1}{r_2^4} \right) \Delta x_2 \cos \theta_2 \right] \quad (\text{A8})$$

in which  $A_{\text{eff}}/A$  is introduced to account for the increase in velocity experienced by the baffle due to induced velocity from vortices from previous cycles. This was obtained as shown in figure 4 by taking the ratio of the observed amplitude of the vortex at the zero velocity point and dividing it by the double amplitude at infinity. By this method, the drag coefficients obtained for  $A/w = 0.33$  were 51 for sinusoidal motion and 33 for slosh motion. For  $A/w = 1$ , 36 was obtained for sinusoidal motion and 32 for slosh motion. These values are reasonably consistent with maximum drag coefficients given in reference 10, which varied from 30 to 40 for  $A/w = 4.2$ .

Because of the approximations involved, equation (A8) should not be expected to give accurate measurements of  $C_D$ , but it should be expected to give values proportional to the damping effectiveness. With this assumption, the ratios of drag coefficients for slosh to sinusoidal motion were used to estimate the drag coefficient in the transition region. The drag coefficients obtained from reference 8 for a 3-inch plate with an oscillation period of 1 sec were multiplied by these ratios to obtain the estimated drag coefficient curve in figure 6.

## REFERENCES

1. Silveira, Milton A.; Stephens, David G.; and Leonard, H. Wayne: An Experimental Investigation of the Damping of Liquid Oscillations in Cylindrical Tanks With Various Baffles. NASA TN D-715, 1961.
2. Abramson, H. Norman; and Garza, Luis R.: Some Measurements of the Effects of Ring Baffles in Cylindrical Tanks. J. Spacecraft and Rockets, vol. 1, Sept.-Oct. 1964, pp. 560-562.
3. Abramson, H. Norman, ed.: The Dynamic Behavior of Liquids in Moving Containers. NASA SP-106, 1966.
4. Miles, J. W.: Ring Damping of Free Surface Oscillations in a Circular Tank. J. Appl. Mech., vol. 25, no. 2, June 1958, pp. 274-276.
5. Cole, Henry A., Jr.; and Gambucci, Bruno J.: Measured Two-dimensional Damping Effectiveness of Fuel-Sloshing Baffles Applied to Ring Baffles in Cylindrical Tanks. NASA TN D-694, 1961.
6. O'Neill, J. P.: An Experimental Investigation of Sloshing. Final Report TR-59-0000-09960, Space Technology Labs., Inc., March 1960.
7. Stephens, David G.; and Scholl, Harland F.: Effectiveness of Flexible and Rigid Ring Baffles for Damping Liquid Oscillations in Large-Scale Cylindrical Tanks. NASA TN D-3878, 1967.
8. Cole, Henry A., Jr.: On a Fundamental Damping Law for Fuel Sloshing. NASA TN D-3240, 1966.
9. Buchanan, Harry: Drag on Flat Plates Oscillating in Incompressible Fluids at Low Reynolds Numbers. NASA TM X-53759, 1968.
10. Keulegan, G. H.; and Carpenter, L. H.: Forces on Cylinders and Plates in an Oscillating Fluid. Natl. Bur. Std. Rep. 4821, Sept. 1956.
11. Cole, Henry A., Jr.: Baffle Thickness Effects in Fuel Sloshing Experiments. NASA TN D-3716, 1966.
12. Stephens, David G.; Leonard, H. Wayne; and Perry, Tom W., Jr.: Investigation of the Damping of Liquids in Right-Circular Cylindrical Tanks, Including the Effects of a Time-Variant Liquid Depth. NASA TN D-1367, 1962.
13. Cole, Henry A., Jr.; and Gambucci, Bruno J.: Tests of an Asymmetrical Baffle For Fuel Sloshing Suppression. NASA TN D-1036, 1961.
14. Durand, W. F., ed.: Aerodynamic Theory, Vol. III. Berlin, Springer, 1934-36.

15. Von Kármán, T. H.; and Sears, W. R.: Airfoil Theory for Nonuniform Motion. J. Aero. Sci., vol. 5, no. 10, Aug. 1938, pp. 379-390.
16. Schwind, R.; Scotti, R.; and Skogh, J.: Analysis of Flexible Baffles for Damping Tank Sloshing. Preprint 66-97, AIAA, 1966.

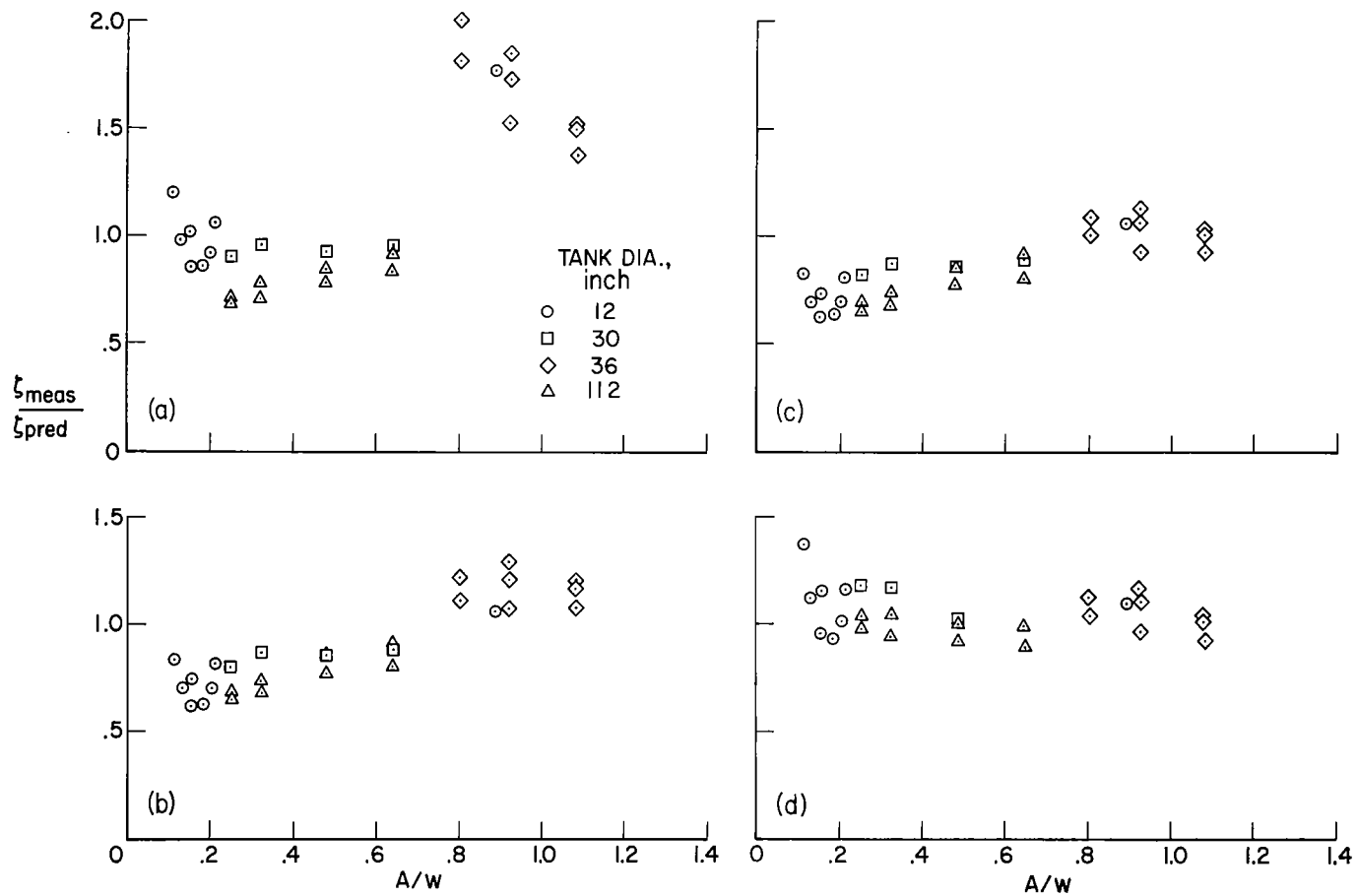
TABLE 1.- EXPERIMENTAL DATA

[Wave decay method]

Tank	2a (in.)	w/a	d/a	$y_s/a$	A/w	$\zeta_{meas}$	$\zeta_o$
Delaurier <sup>a</sup>	11.45	0.083	0.466	0.098	0.89	0.0145	0.0055
Reference 6	11.9	.125	.505	.032	.20	.0055	.0019 <sup>b</sup>
	↓	↓	↓	.023	.15	.0052	↓
	↓	↓	↓	.017	.11	.0052	↓
	↓	↓	↓	.034	.21	.0065	↓
	↓	↓	↓	.028	.18	.0047	↓
	↓	↓	↓	.024	.15	.0044	↓
Reference 7	30	.1	.3	.021	.13	.0047	.001 <sup>b</sup>
	↓	↓	↓	.0216	.25	.0083	↓
	↓	↓	↓	.0276	.32	.0099	↓
	↓	↓	↓	.0415	.48	.0118	↓
Reference 11	36	.083	.33	.0552	.64	.014	.0035
t/w = 0 and 0.042	↓	↓	↓	.0834	1.08	.0165	↓
	↓	↓	↓	↓	↓	.018	↓
	↓	↓	.42	↓	.92	.0183	↓
	↓	↓	↓	↓	↓	.0123	↓
	↓	↓	↓	↓	↓	.015	↓
	↓	↓	.5	↓	.8	.014	↓
	↓	↓	↓	↓	↓	.011	↓
Reference 7	112	.1	.3	.0216	.25	.010	.0003 <sup>b</sup>
	↓	↓	↓	.0276	.32	.0062	↓
	↓	↓	↓	.0415	.48	.0073	↓
	↓	↓	↓	.0552	.64	.0108	↓
	↓	↓	.4	.026	.25	.0135	↓
	↓	↓	↓	.0334	.32	.0046	↓
	↓	↓	↓	.05	.48	.0056	↓
	↓	↓	↓	.0667	.64	.0070	↓
	↓	↓	↓	↓	↓	.0084	↓

<sup>a</sup>Unpublished Ames tests by James Delaurier.

<sup>b</sup>Estimated from reference 12.



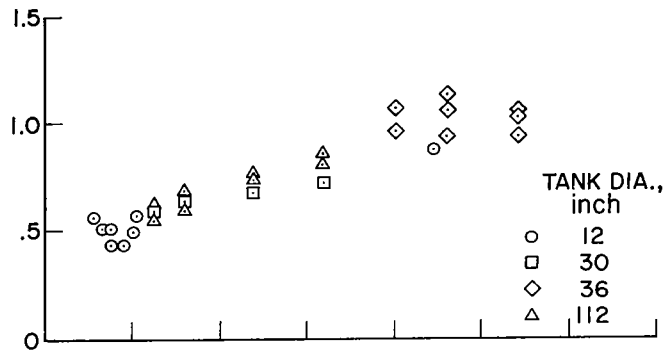
(a) Miles equation.

(b) Wall damping included.

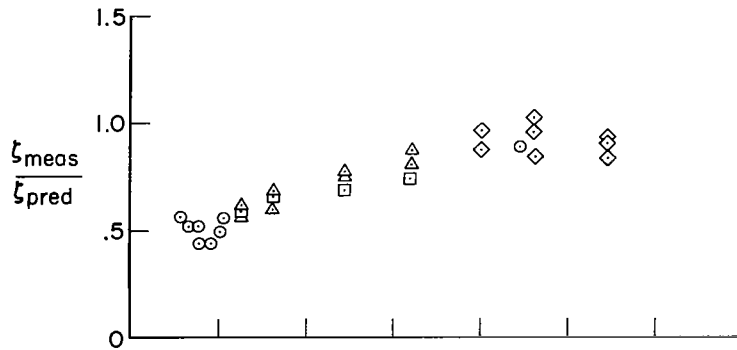
(c) Wall damping and generalized mass factors included.

(d) Wall damping, generalized mass, and vortex shedding factors included.

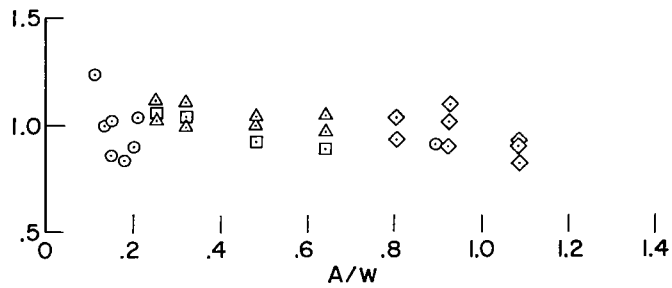
Figure 1.- Comparison of predicted damping by Miles' equation with measurements in table 1.



(a) NASA TN D-3240 (includes wall damping).



(b) Generalized mass factors included.



(c) Generalized mass and vortex shedding factors included.

Figure 2.- Comparison of predicted damping by NASA TN D-3240 with measurements in table 1.

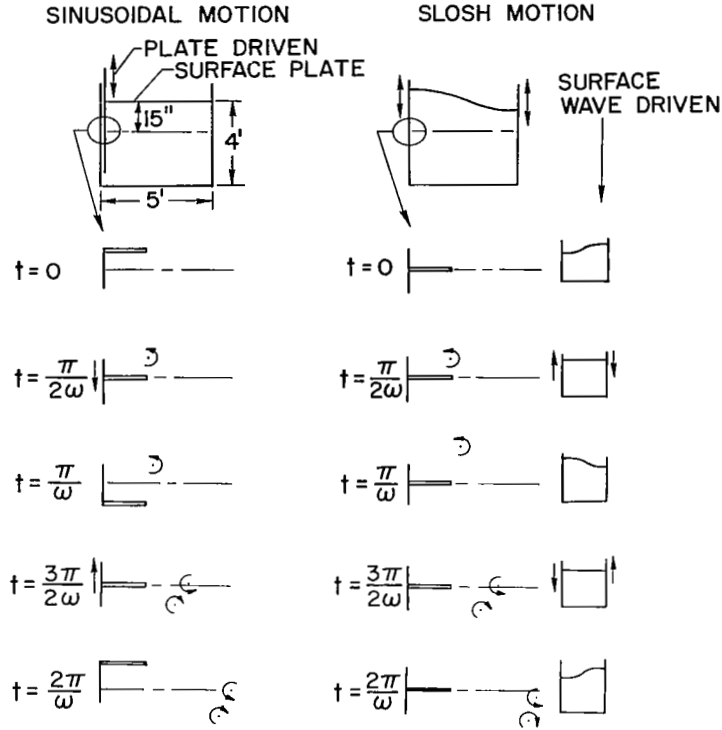
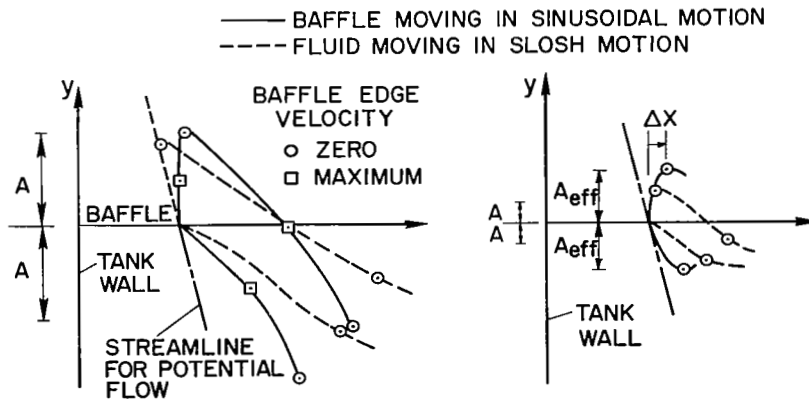
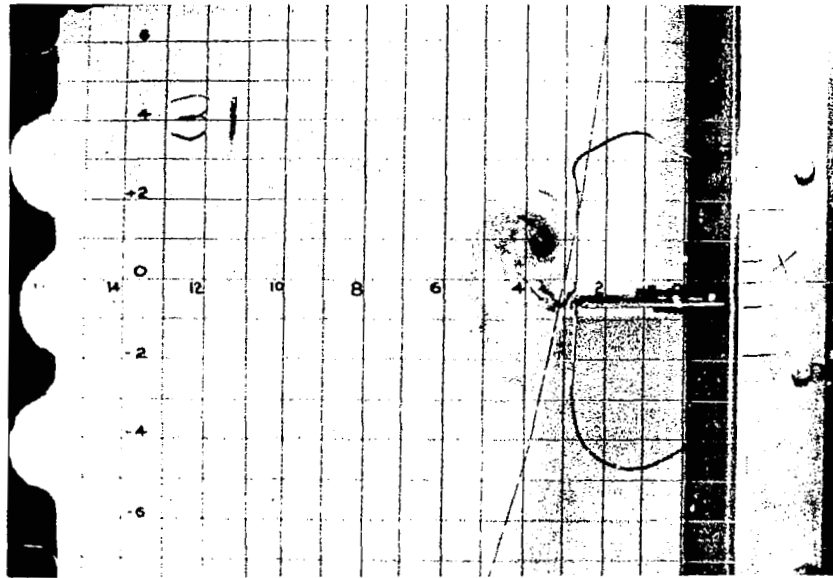


Figure 3.- Experimental method used to obtain two forms of motion and schematic drawing of vortex locations at various times over one cycle of oscillation.

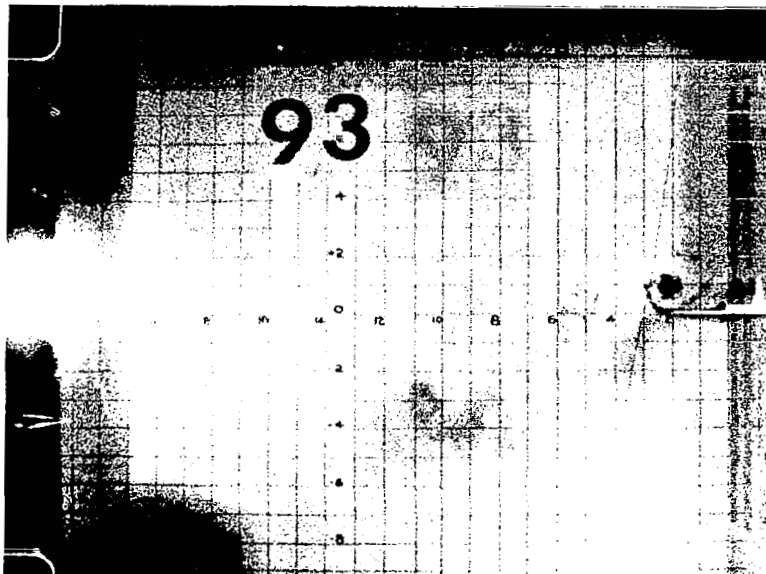


(a)  $A/w = 1$ ,  $Re = 16 \times 10^3$       (b)  $A/w = 0.33$ ,  $Re = 5 \times 10^3$

Figure 4.- Comparison of vortex path relative to baffle for sinusoidal motion and slosh motion in a rectangular tank;  $d/a = 0.5$ ,  $t/w = 0.02$ .

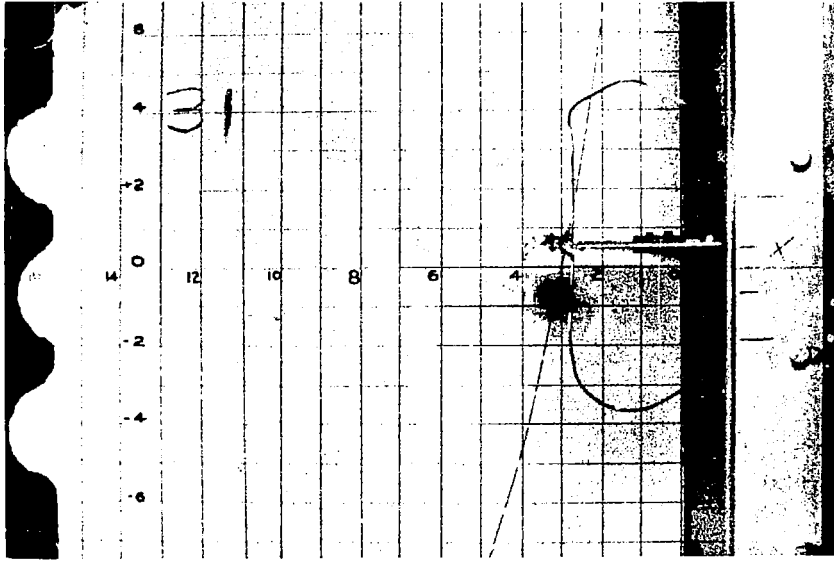


(a) Sinusoidal motion  $t = \pi/\omega$ .

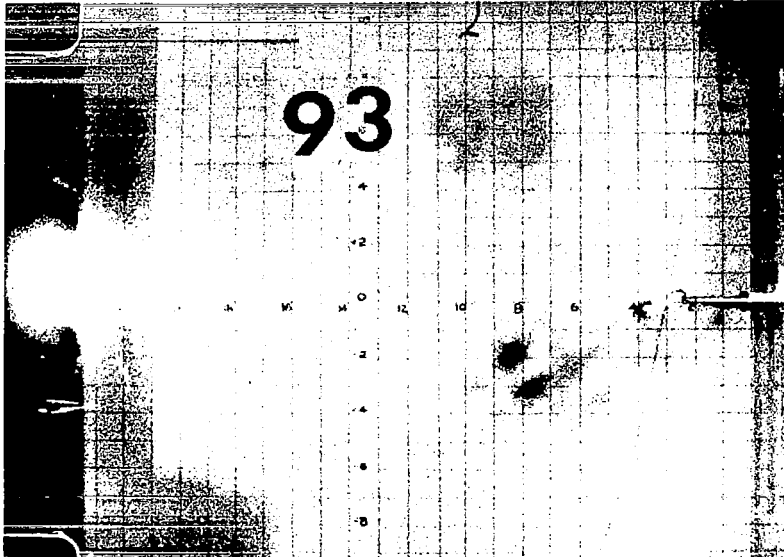


(b) Slosh motion  $t = \pi/\omega$ .

Figure 5.- Effect of motion on flow pattern for  $A/w = 0.33$ .

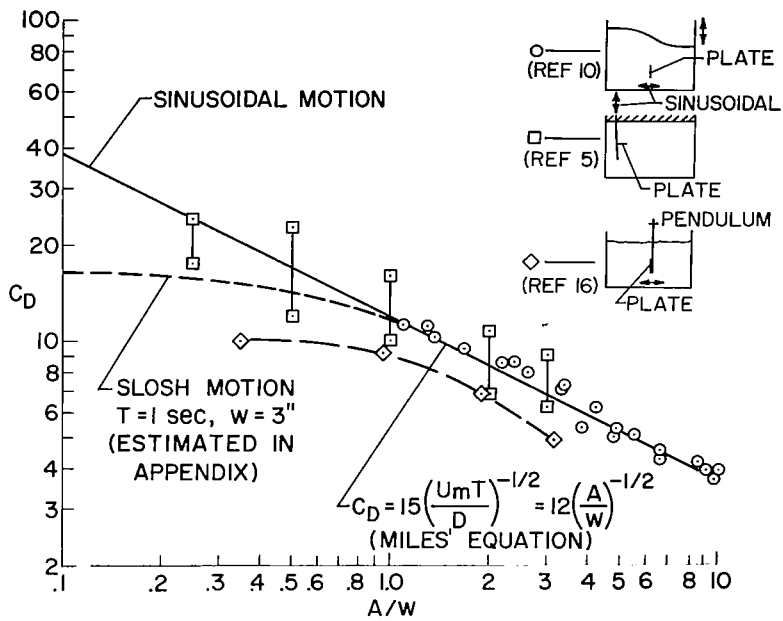


(c) Sinusoidal motion  $t = 2\pi/\omega$ .

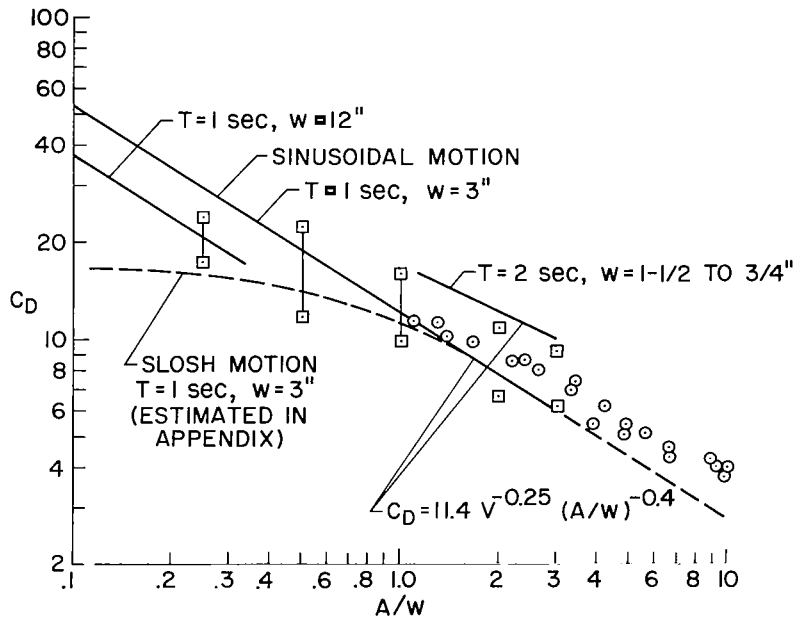


(d) Slosh motion  $t = 2\pi/\omega$ .

Figure 5.- Concluded.



(a) Reference 4 (Miles).



(b) Reference 8 (TN D-3240).

Figure 6.- Comparison of measured two-dimensional drag coefficients with empirical relations used for prediction of damping in cylindrical tanks.

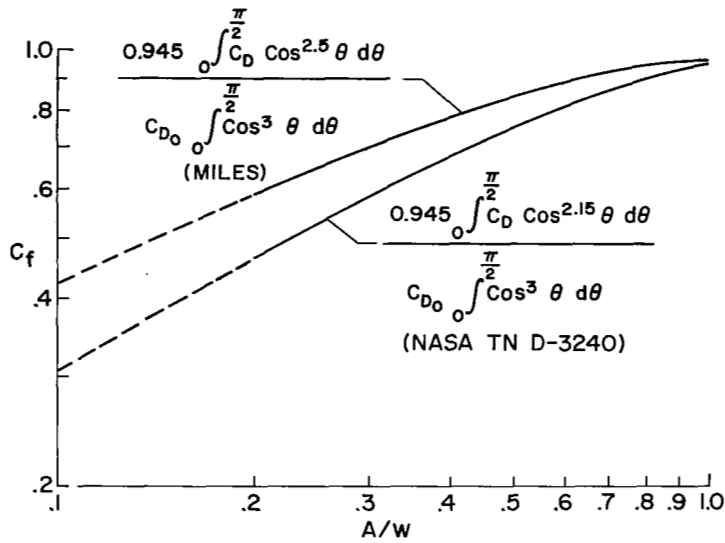


Figure 7.- Correction factor for damping ratio of cylindrical tanks obtained by integrating  $C_D$  around the ring including correction for approximation in  $y/y_s$ .

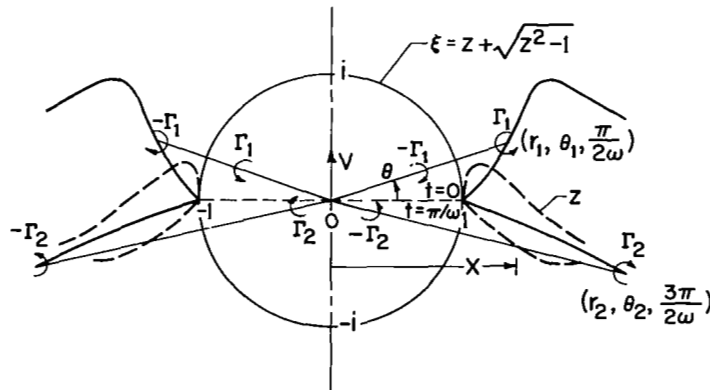
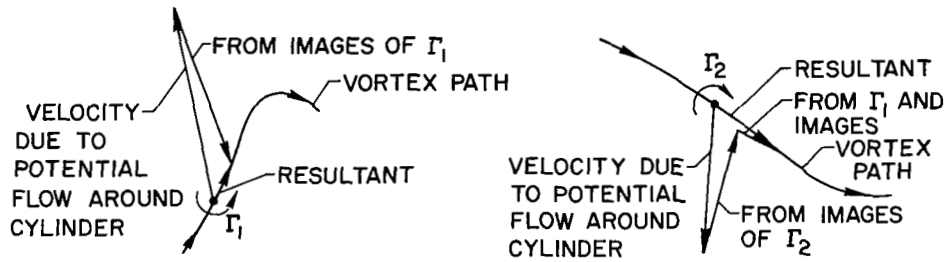


Figure 8.- Conformal transformation of plate and vortex paths into unit circle and vortices and images.



(a) Resolution of velocity vectors at  $r_1, \theta_1, \pi/2\omega$ . (b) Resolution of velocity vectors at  $r_2, \theta_2, 3\pi/2\omega$ .

Figure 9.- Determination of circulation for nonsymmetrical case.

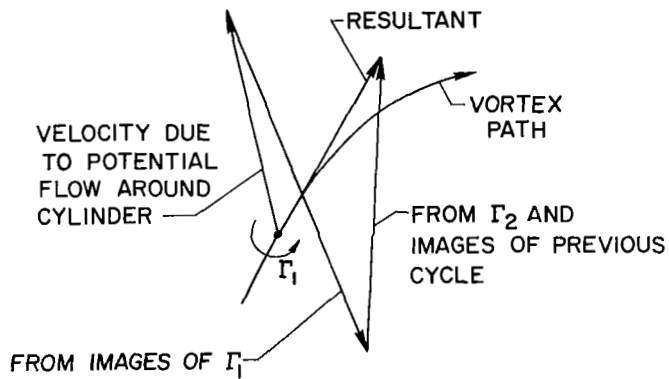


Figure 10.- Determination of circulation for symmetrical case  $\Gamma_1 = \Gamma_2$ .